Journal of Energy Storage 22 (2019) 194–207

Contents lists available at ScienceDirect

Journal of Energy Storage

journal homepage: www.elsevier.com/locate/est

Combined electrical and electrochemical-thermal model of parallel connected large format pouch cells

Elham Hosseinzadeh, James Marco*, Paul Jennings

WMG, University of Warwick, Coventry, CV4 7AL, United Kingdom

ARTICLE INFO

Keywords:
Load imbalance
Large format cells
Battery pack
Capacity loss
Parallel connected cells
Co-simulation

ABSTRACT

Variation in energy capacity and resistance of cells connected in parallel can degrade the overall performance of the energy storage system (ESS). Such variations can lead to significant individual differences in battery load current, state of charge (SOC) and heat generation. An experimentally validated 1D electrochemical-thermal model of a large format 53 Ah pouch cell is employed to underpin the performance evaluation of parallel connected cells within the context of a complete ESS. The cell model, developed within COMSOL Multiphysics is coupled with an electrical circuit model of the ESS within Matlab. Results are presented that quantify cell-to-cell differences in load current and heat generation as the length of the parallel connection and value of the cell interconnection resistance is varied. The results highlight that variations in cell depth of discharge and the occurrence of temperature gradients across the parallel connection increases at higher load currents and interconnect resistances. The impact is amplified as the length of the parallel connection increases which will accelerate cell ageing and, if unmanaged, may present safety concerns.

1. Introduction

In the recent years, lithium ion batteries have grown in popularity for use within electric vehicles (EVs) and hybrid electric vehicles (HEVs) due to their relatively high energy and power densities compared to other battery technologies [48,49]. However, a number of studies have highlighted the challenge of commercialising the technology, such as the need to address component cost, reliability and safety [1]. The performance of electrified vehicles strongly depends on the electrical characteristics of the battery pack within the powertrain [2,3]. The energy storage system (ESS) will often comprise a large number of cells, electrically connected in both series and parallel to achieve the desired voltage, energy density and power capability required for the vehicle [4]. Research has highlighted that variations among cells within a single ESS (e.g. energy capacity and internal resistance) and the resulting differences in battery state of charge (SOC) and temperature, are the primary factors for battery aging [5–7], with SOC noted as having the greatest impact [8,9]. Cell to cell variations originate from either battery manufacturing inconsistencies [5,8,10,11], extended periods of storage [12] or through electrical loading within a heterogeneous environment in which cells are subject to different electrical currents and ambient temperatures [10].

Cells connected in series within an ESS experience a common applied current. However, depending on the system design of the ESS and the cell characteristics, each cell may have a different terminal voltage and operate at a different temperature. The level of temperature variation will largely depend on the design of the thermal management system (TMS) and the magnitude of the applied current. As discussed within [13], an uneven temperature distribution between cells leads to a further mismatch of internal resistance. As the cut-off voltage is defined by the weakest cell within the series connection, this phenomena will negatively affect overall capacity [11,14]. As reported within [15], a temperature variation of 15 °C between the cells can lead to a 5% overall capacity reduction within the ESS. Conversely, cells connected in parallel will have a common terminal voltage but will typically undergo different load currents. The unequal loads are due to the combined effect of variations in capacity and resistance and due to differences in interconnect resistance. These attributes (in isolation or when combined) lead to a further mismatch of internal resistance, temperature and SOC among the cells. This, in turn, results in a further divergence in the electrical loading of each cell and is known to accelerate cell aging and system degradation [4,13]. This inconsistency is not typically monitored within the battery management systems (BMS), as the BMS does not have access to the properties of individual cells and the financial cost and resulting complexity of installing a current sensor within each parallel electrical path of the ESS would be prohibitive

* Corresponding author.
E-mail address: James.Marco@warwick.ac.uk (J. Marco).

https://doi.org/10.1016/j.est.2019.02.004
Received 19 September 2018; Received in revised form 28 November 2018; Accepted 3 February 2019

Nomenclature

List of symbols

a_s	reaction surface area
$brugg_n$	Bruggeman porosity exponent
C	Li^+ concentration ($mol\,m^{-3}$
D	diffusion coefficient ($m^2\,s^{-1}$)
E_{act}	activation energy
F	Faraday's constant ($C\,mol^{-1}$)
$f_{\pm}$	electrolyte activity coefficient
h	heat transfer coefficient ($W/(m^2\,K)$)
I	current load (A)
I_{pair}	current of a single-pair electrode (A)
i_0	exchange current density ($A\,m^{-2}$)
j^{Li}	reaction current density ($A\,m^{-2}$)
k_i	reaction rate ($m^{2.5}\,mol^{-0.5}\,s^{-1}$)
L	thickness of the electrode (μm)
N_{pairs}	number of electrode-pairs
R_{cell}	internal resistance of the cell (Ω)
R_{IC}	interconnect resistance between the cells (Ω)
R_{SEI}	resistance of the SEI layer ($\Omega\,cm^{-2}$)
R_{uni}	universal gas constant ($J\,mol^{-1}\,K^{-1}$)
r	radial coordinate in spherical particle (μm)
r_p	particle radius (μm)
T	temperature (°C)
t	time (s)
t_+^0	transference number
$U_{ref,i}$	open circuit potential of the electrodes
V_t	terminal voltage
x	local state of charge of the negative electrode
y	local state of charge of the positive electrode

Greek letters

α	symmetry factor
δ_{cell}	capacity of a cell (Ah)
ε	volume fraction
η	overpotential (V)
k_D^{eff}	diffusional conductivity ($S\,m^{-1}$)
σ	electronic conductivity ($S\,m^{-1}$)
κ	ionic conductivity ($S\,m^{-1}$)
ϕ	potential (V)
ψ	a general parameter

Subscripts/superscripts

a	anode
amb	ambient
c	cathode
cc	current collector
e	electrolyte
eff	effective
f	filler
neg	negative
pos	positive
s	solid
sep	separator
surf	surface
x	direction through the cell thickness
z	direction along the cell height

Terms and abbreviation

Al	aluminium
Cu	copper
exp	experimental
OCV	open circuit voltage
sim	simulation
SOC	state of charge

[47,50]. A typical BMS assumes that all the cells connected in parallel have the same State of Health (SoH) and SOC due to their common terminal voltage. This assumption may result in further degradation and over-charging/discharging hazards for individual cells [6]. Such scenarios have already been discussed within the literature [1,4,13,16].

A consensus does not yet exist as to the optimal design of battery cell, in terms of both chemistry and form-factor, for use within automotive applications. The integration challenge associated with designing a complete ESS using either large format pouch cells or smaller cylindrical cells are reported within [17,18]. Currently, a number of EVs (such as the Tesla Model S and Roadster) use small capacity (e.g. 2–5 Ah), cylindrical cells. Conversely, vehicles such as the Nissan leaf, Renault Zoe, BMW i-3 and BMW ActiveE employ larger format batteries that have a higher energy capacity (e.g. 20–35 Ah) [19,20]. Many publications advocate the use of small cylindrical cells, citing their relative low cost and wide availability [21,22], the quality of the manufacturing processes and therefore the reduced manufacturing variations often observed [14,23]. The integration of smaller cells within the ESS results in higher number of cells connected in parallel (to meet the application energy and power requirements). The disadvantage of this approach is potentially high complexity in the system design, with an increased number of failure modes and possibly higher manufacturing cost [24,25]. An ESS aggregated from larger format cells with a greater energy and power density, arguably requires fewer cells connected in parallel to meet vehicle performance targets of driving range and acceleration. Despite the potential advantages associated with the use of large format cells, they equally impose some challenges to the overall ESS design [26]. Their larger physical size implies the presence of temperature gradients across the cell surface are more likely, increasing the possibility of localised degradation and the possible onset of thermal runaway [27–30].

Due to the interdependency of cell internal impedance to load current, battery SOC and temperature, a coupled electrochemical-thermal model for characterising the performance of a battery cell and battery pack is necessary, especially when having large format batteries dealing with high charge and discharge rates [4]. Wu et al. [4] used a P2D electrochemical model to investigate the impact of interconnect resistance on the load imbalance of a 8P1S battery pack using 6 Ah LCO cylindrical cells. The authors identified that cyclic or pulsed loads result in considerable temperature inhomogeneity within a pack, while it is less significant for constant current excitation. It is noteworthy that the authors do not include a thermal management model within their analysis, which would in practice impact the level of the temperature inhomogeneity observed within the complete system. Within their research, cell resistance was assumed constant.

This research aims to extend previous studies [4,10,17] that have employed a simplified model of battery cells connected electrically in parallel in which the cell resistance is assumed constant. The scope of this study is the derivation of a battery system model underpinned by the integration of a previously validated electrochemical thermal cell model that clearly shows the dependency between cell resistance, temperature and SOC. The motivation for this research is the creation of a model that will facilitate future research into novel battery pack architectures and thermal management designs, with an emphasis on the

use of parallelised large format cells to achieve the required values of energy density and power capability of the ESS. The novelty of this model in relation to previous studies is that it takes account of the interdependency between cell capacity, resistance, SOC and temperature. Different use cases were investigated to highlight the potential for differential current flows within the parallel connection and the potential safety issues and hazards that emerge when using a parallel connection of cells within the battery design.

This paper is structured as follows. Section 2 presents the electrochemical-thermal model of the single cell within COMSOL Multiphysics, including derivation of the model equations, their parameterisation and model validation. Sections 3 and 4 defines the electrical circuit model within Matlab and the creation of a co-simulation environment to facilitate the numerical coupling of the circuit model with the electrochemical-thermal model, thereby producing a simulation of the complete ESS. Results are presented in Section 5 that quantify cell-to-cell differences in load current and heat generation as the length of the parallel connection and value of the cell interconnection resistance is varied. Section 6 and Section 7 present Further Work and Conclusions respectively.

2. Electrochemical-thermal cell model

2.1. Model derivation

A 1-D electrochemical-thermal model of a 53 Ah pouch cell with NMC – Graphite chemistry (manufactured by XALT ENERGY), based on a Pseudo Two-Dimensional (P2D) battery model was developed within the COMSOL Multiphysics software package. The structure of the cell and model domain includes one electrode pair (negative current collector, negative electrode, separator, positive electrode, positive current collector) through the thickness of the cell and is displayed in Fig. 1(a) and (b). By solving for charge, mass and energy conservation, as well as electrochemical kinetics implemented in a P2D model the five main variables are found, namely: lithium concentration in the solid (C_s), and electrolyte phase (C_e), potential in the solid (ϕ_s) and electrolyte phase (ϕ_s) as well as volumetric reaction current (j_{Li}). Additional model outputs include but are not constrained too: terminal voltage (V_t), battery SOC, heat generation (Q) and temperature (T). A full derivation of the electrochemical model, including the underpinning assumptions has already been published in [31–33] for a 10 Ah LFP and a 53 Ah NMC pouch cell respectively, and will therefore not be repeated here. However, the state and algebraic equations including boundary conditions are provided in Table 1 for completeness.

The physical values required to parameterise the cell model were extracted through a comprehensive set of experiments that includes a battery tear-down and the use of scanning electron microscopy (SEM) to quantify the number of layers, the thickness and dimensions of each layer and the particle sizes for the different materials employed in cell construction. A further set of experiments was undertaken to define the dynamic parameters of the cell, such as the reaction rate (k_i), and the activation energies for temperature dependent parameters (e.g. $E_{act,\psi}$) within the Arrhenius function. Those include the open circuit voltage (OCV) measurements and energy capacity test including charge and discharge under different C-rates at 5–45 °C ambient temperatures. Table 2 presents the full set of electrochemical parameters employed within this study. A complete description of the methodology employed to both parameterise and validate the cell model is discussed within [33] and will therefore not be repeated here.

2.2. Model validation

The developed cell model was extensively validated against constant charge (0.5–2C) and discharge current rates (0.5–5C) at different ambient temperatures (5–45 °C). Such a test protocol was necessary to quantify the correlation between the battery internal resistance and the combined effect of load current, SOC and temperature. A natural convection boundary condition with h value of 6 W/(m^2 K) provided the best fit to the experimental data. The full verification methodology is explained within [33] and will therefore not be repeated here. A subset of the validation in [33] is presented in Fig. 2 for completeness. Fig. 2 shows the validation of the model against experimental data under the WLTP class 3 drive-cycle (Worldwide Harmonised Light Vehicle Test Procedure (WLTP)), at different ambient temperatures.

The initial SOC employed at the start of the simulation was 100%. At the end of the drive-cycle SOC has reduced to 5%. Experimental measurements (contained within [33]) confirm that the cell has a relatively poor performance at low temperatures, in the order of 5 °C, resulting in a higher heat generation and consequently a higher temperature rise. By increasing the ambient temperature from 5 to 25 °C cell electrical performance was observed to significantly improve (the increased cell voltage leads to reduced heat generation; almost half of that observed at a temperature of 5 °C). However, by further increasing ambient temperature, the performance of the cell does not change significantly and the total heat decreases by circa 19%. The validation tests show that cell model accuracy is within 12.1% peak and 1.2% average error at 5 °C. The error significantly reduces as the ambient temperature rises, down to 5.3% and 2.7% peak error at 25 °C and 45 °C respectively. The corresponding average error is much less, equal to 0.8% and 0.7% at 25 °C and 45 °C respectively. As it can be seen, the peak error increases as SOC reduces, especially within the region of SOC < 20%. The model accuracy is comparable with a study published by Farag et al. [38], in which a broad range of operating conditions was addressed. The maximum surface temperature of the cells, measured by 8 temperature sensors (distributed over the cell surface) at the end of the cycle reaches to 21.2 °C, 34.5 °C and 52.4 °C at 5 °C, 25 °C and 45 °C

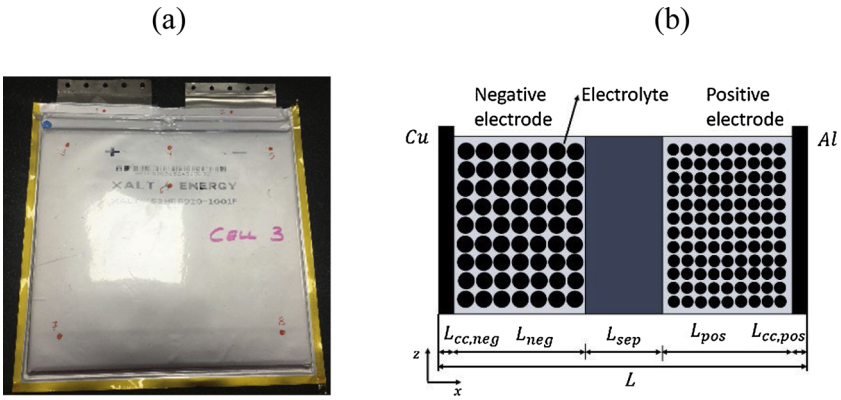

Fig. 1. (a) Photograph of the 53 Ah cell manufactured by XALT ENERGY, (b) The representative domain for the coupled 1D electrochemical-thermal model (through the thickness of the cell).

Table 1
Governing equations and boundary conditions for the P2D modelling framework [33].

Description	Governing equations	Boundary conditions	
Current of one electrode pair	$I_{pair} = \frac{\delta_{cell} \cdot C\text{-}rate}{N_{pairs}}$		(1)
Mass conservation: lithium in the solid phase	$\frac{\partial(C_s)}{dt} = \frac{D_s}{r^2}\frac{\partial}{\partial r}\left(r^2\frac{\partial C_s}{\partial r}\right)$	$\frac{\partial C_s}{\partial r}\Big\|_{r=0} = 0$ $-D_s\frac{\partial C_s}{\partial r}\Big\|_{r=r_p} = \frac{j^{Li}}{a_s F}$	(2)
Mass conservation: lithium in the electrolyte phase	$\frac{\partial(\varepsilon_e C_e)}{dt} = \nabla.(D_e^{eff}\nabla C_e) + \frac{1-t_+^0}{F}j^{Li}$	$\frac{\partial C_e}{\partial x}\Big\|_{x=L_{cc,neg}} = 0$ $\frac{\partial C_e}{\partial x}\Big\|_{x=L-L_{cc,pos}} = 0$	(3)
Electronic charge balance: potential in the solid phase	$\nabla(\sigma^{eff}\nabla\phi_s) = j^{Li}$	$\phi_{cc}\|_{x=0} = 0$ $-\sigma_{cc}\nabla\phi_{cc}\|_{x=L} = -I_{pair}$ $\nabla\phi_s\|_{x=L_{cc,neg}+L_{neg}} = 0$ $\nabla\phi_s\|_{x=L_{cc,neg}+L_{neg}+L_{sep}} = 0$	(4)
Electronic charge balance: potential in the electrolyte phase	$\nabla(k^{eff}\nabla\phi_e) + \nabla(k_D^{eff}\nabla\ln C_e) + j^{Li} = 0$	$\frac{\partial\phi_e}{\partial x}\Big\|_{x=L_{cc,neg}} = 0$ $\frac{\partial\phi_e}{\partial x}\Big\|_{x=L-L_{cc,pos}} = 0$	(5)
Electrochemical kinetics: reaction current density	$j^{Li} = a_s i_0\left\{\exp\left[\frac{\alpha_a F}{R_{uni}T}\eta\right] - \exp\left[-\frac{\alpha_c F}{RT}\eta\right]\right\}$		(6)
Reaction surface area	$a_s = \frac{3\varepsilon_s}{r_P} = \frac{(1-\varepsilon_e-\varepsilon_f)}{r_p}$		(7)
Exchange current density	$i_0 = k_i(C_e)^{\alpha a}(C_{surf,max} - C_{surf,e})^{\alpha a}(C_{surf,e})^{\alpha c}$		(8)
Overpotential	$\eta_i = \phi_{s,i} - \phi_{e,i} - U_{ref,i}$		(9)

respectively. Moreover, the corresponding temperature rise of the cell surface is equal to 16.2, 9.5 and 7.4 °C. Based on the validation results presented in Table 3, the 1D electrochemical-thermal model of the NMC lithium-ion pouch cell was deemed to be sufficiently accurate to justify its use within this study and therefore to underpin the derivation of the complete ESS model.

3. Electrical model

The electrical load imbalance that arises within a parallel connection of cells due to variations in cell interconnect resistance, is especially noticeable within large battery packs [4]. A schematic of a (1S 5P) ESS is presented in Fig. 3(a). The 1S 5P configuration was deemed to yield sufficiently representative results to highlight the challenges of connecting cells in parallel, while concurrently resulting in a model that was computationally efficient to underpin a range if diffident simulation studies. It is noteworthy, that a parallel connection of five 53 Ah cells contains the same energy capacity as the 74 3.1 Ah cells that are connected electrical in parallel within the battery module employed within the Tesla Model S. As it can be seen, the external load is applied as a current source (I_{load}). The first cell ($Cell_1$) is connected to the terminals of the ESS with the remainder of cells ($Cell_{2-5}$) connected together via a network of resistances ($R_{IC,n}$). Based on Kirchhoff's current law, the sum of the currents at each junction equals zero. As shown in Fig. 3(b), the relationship between the loop current and the individual cell currents can be described as follows. It is noteworthy that the following generalised equations are valid for the assumption that the interconnect resistances are equal within the system ($R_{IC,i} = R_{IC}$).

$$I_{cell,n} = \begin{cases} I_n - I_{n+1}, & n < N \\ I_n, & n = N \end{cases} \tag{20}$$

Similarly, from Kirchhoff's voltage law, the voltages around each loop sum to zero.

$$V_{t,n} - V_{t,n-1} + 2R_{IC}I_n = 0 \tag{21}$$

The parameter N defines the number of cells connected electrically in parallel within the battery system.

The characteristics of each cell are represented within the circuit model by the validated electrochemical-thermal model (described in Section 2). Within the context of the electrical circuit, each cell represents a variable voltage source in series with a variable resistor. Within many studies, such as [39], the cell resistance is assumed to be constant. This assumption limits the validity and usefulness of the model, especially when studying the operation of EVs that may exercise the battery over a wide SOC range and for SOC values below circa 20% where cell resistance is known to increase rapidly and be highly non-linear [40]. Within this model, the dynamic behaviour of the cell resistance as a function of battery current, SOC and temperature is considered within the coupled COMSOL model. Terminal voltage of the cell can be defined as:

$$V_t = OCV + R_{cell}I_{cell} \tag{22}$$

By substituting V_t in Eq. (21), the following equation is extracted.

$$\begin{cases} OCV_n - OCV_{n-1} + R_{cell,n}(I_n - I_{n+1}) - R_{cell,n-1}(I_{n-1} - I_n) + 2R_{IC}I_n = 0, & n < N \\ OCV_n - OCV_{n-1} + R_{cell,n}I_n - R_{cell,n-1}(I_{n-1} - I_n) + 2R_{IC}I_n = 0, & n = N \end{cases} \tag{23}$$

The aforementioned equation can be written in matrix form as:

$$R\begin{bmatrix} I_1 \\ I_2 \\ I_3 \\ I_4 \\ I_5 \end{bmatrix} = A\,OCV + B\,I_{load} \tag{24}$$

Table 2
The electrochemical parameters of the 53 Ah pouch cell with NMC chemistry [33].

Parameters	Negative electrode	Separator	Positive electrode
Constant parameters			
Bruggeman porosity exponent, $brugg_n$	1.5 [4,34]		
Universal gas constant, R_{uni}	8.314		
Faraday's constant, F	96,485		
Design specification			
Thickness, L (μm)	74.83[a]	17[a]	41.16 [a]
Particle size, r_p (μm)	26.2[a]		10.7[a]
Volume fraction of the active material, ε_s	0.58 [34]		0.43 [34]
Volume fraction of the electrolyte, ε_e	0.32 [34]	0.54 [34]	0.32 [34]
Maximum lithium concentration in the solid phase, $C_{s,max}$ (mol m^{-3})	29,802[b]		87,593[b]
Electrolyte lithium concentration, $C_{e,max}$ (mol m^{-3})		1200 [4,34]	
Stoichiometry at SOC = 1, x_1, y_1	0.75[b]		0.38[b]
Stoichiometry at SOC = 0, x_0, y_0	0.05[b]		0.93[b]
R_{SEI} (Ω cm^2)	20		20
Lithium ion transference number, t_+^0	0.363	0.363	0.363
Electrolyte activity coefficient, $f_\pm$	1 [4]	1 [4]	1 [4]
Charge transfer coefficient, α	0.5 [4]		0.5 [4]
Dynamic parameters			
Lithium diffusion coefficient in the negative electrode, $D_{s,neg}$ (m^2 s^{-1})	$D_{s,neg} = 3\times10^{-13}\exp\left(\frac{-35000}{R_{uni}}\left(\frac{1}{T}-\frac{1}{298.15}\right)\right)^2$		(10)
Lithium diffusion coefficient in the positive electrode, $D_{s,pos}$ (m^2 s^{-1})	$D_{s,pos} = 7\times10^{-14}\exp\left(\frac{-35000}{R_{uni}}\left(\frac{1}{T}-\frac{1}{298.15}\right)\right)^2$		(11)
Lithium diffusion coefficient in the electrolyte, $D_{s,e}$ (m^2 s^{-1})	$D_e = 3.8037e-10\times\exp(-0.78281C)\exp\left(\frac{-10000}{R_{uni}}\left(\frac{1}{T}-\frac{1}{298.15}\right)\right)$ [35]		(12)
Reaction rate in the negative electrode, k_{neg} (m s^{-1})	$k_{neg,discharge} = 5\times10^{-10}\exp\left(\frac{-20000}{R_{uni}}\left(\frac{1}{T}-\frac{1}{298.15}\right)\right)^2$		(13)
	$k_{neg,charge} = 1.2\times10^{-9}\exp(-5x)\exp\left(\frac{-20000}{R_{uni}}\left(\frac{1}{T}-\frac{1}{298.15}\right)\right)^2$		
Reaction rate in the positive electrode, k_{pos} (m s^{-1})	$k_{pos,discharge} = 2.5\times10^{-10}\exp(-5y)\exp\left(\frac{-20000}{R_{uni}}\left(\frac{1}{T}-\frac{1}{298.15}\right)\right)^2$		(14)
	$k_{pos,charge} = 6\times10^{-10}\exp\left(\frac{-20000}{R_{uni}}\left(\frac{1}{T}-\frac{1}{298.15}\right)\right)^2$		
Electrolyte ionic conductivity, κ (S cm^{-1})	$\kappa = 15.8\times c_e\cdot\exp(-13472Ce^{1.4})\exp\left(\frac{-20000}{R_{uni}}\left(\frac{1}{T}-\frac{1}{298.15}\right)\right)^2$ [4]		(15)
Open circuit potential of the negative electrode	$U_{ref,neg} = 0.6379+0.5416\exp(-305.5309x)+0.044\tanh\left(-\frac{x-0.1958}{0.1088}\right)$ [36]		(16)
	$-0.1978\tanh\left(\frac{x-0.0117}{0.0529}\right)-0.0175\tanh\left(\frac{x-0.5692}{0.0875}\right)$		
Open circuit potential of the positive electrode	$U_{ref,pos} = -10.72y^4+23.88y^3-16.77y^2+2.595y+4.563$ [37]		(17)
Local state of charge of the negative electrode, x	$x = SOC_{neg} = \frac{C_{s,surf,neg}}{C_{s,max,neg}}$		(18)
Local state of charge of the positive electrode, y	$y = SOC_{pos} = \frac{C_{s,surf,pos}}{C_{s,max,pos}}$		(19)

[a] Derived from experimentation.

$$R = \begin{bmatrix} 1 & 0 & 0 & 0 & 0 \\ 0 & -(R_{cell1}+R_{cell2}+2R_{IC}) & R_2 & 0 & 0 \\ 0 & R_2 & -(R_{cell2}+R_{cell3}+2R_{IC}) & R_3 & 0 \\ 0 & 0 & R_3 & -(R_{cell3}+R_{cell4}+2R_{IC}) & R_4 \\ 0 & 0 & 0 & R_4 & -(R_{cell4}+R_{cell5}+2R_{IC}) \end{bmatrix}$$

$$A = \begin{bmatrix} 0 & 0 & 0 & 0 & 0 \\ -1 & 1 & 0 & 0 & 0 \\ 0 & -1 & 1 & 0 & 0 \\ 0 & 0 & -1 & 1 & 0 \\ 0 & 0 & 0 & -1 & 1 \end{bmatrix}$$

$$B = \begin{bmatrix} 1 \\ -R_{cell1} \\ 0 \\ 0 \\ 0 \end{bmatrix}$$

Finally, the relationship between the loop current and external load current can be evaluated as:

$$\begin{bmatrix} I_1 \\ I_2 \\ I_3 \\ I_4 \\ I_5 \end{bmatrix} = R^{-1}(A\,OCV + B\,I_{load}) \tag{25}$$

Once the individual loop currents are defined, the cell currents can be

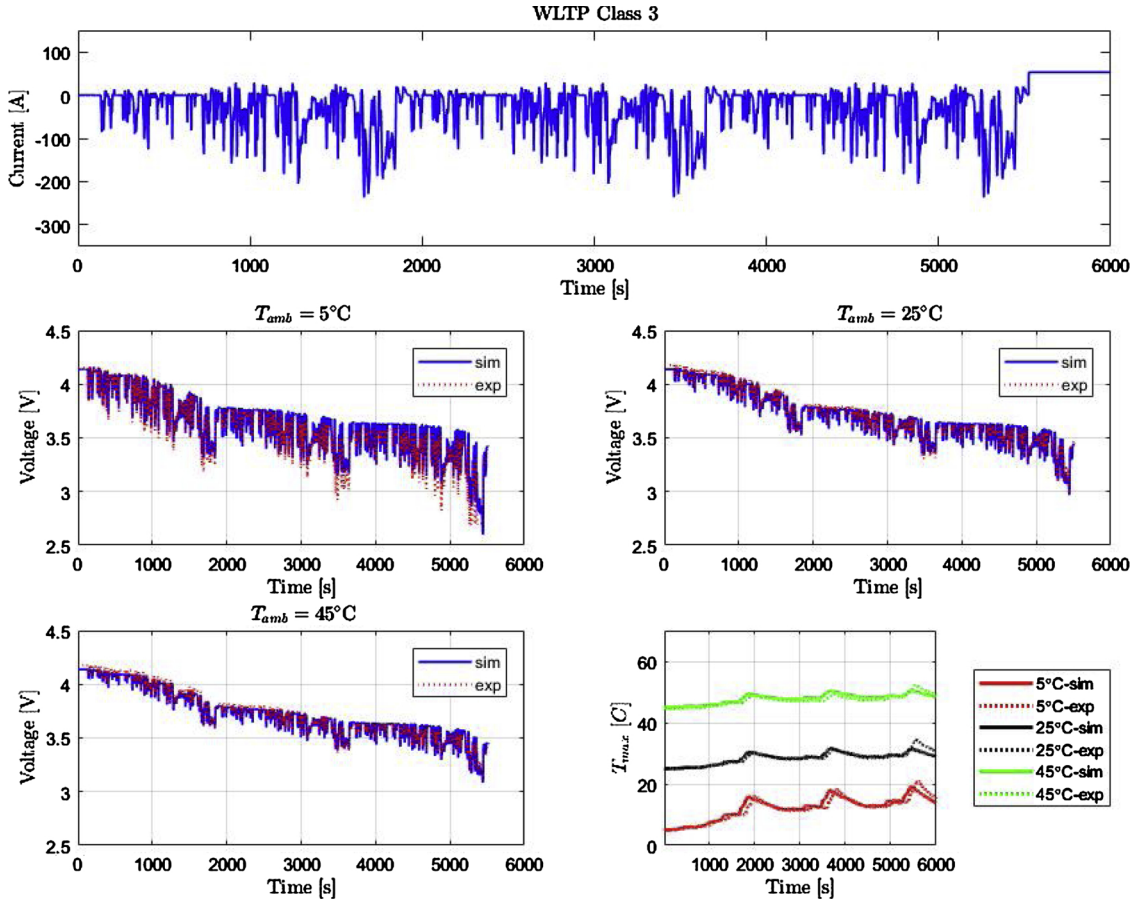

Fig. 2. Model verification under WLTP class 3 drive cycle at 5 °C, 25 °C and 45 °C.

Table 3
The peak and average error of the model for the voltage and temperature prediction of the cell during the WLTP class 3 drive cycle at 5 °C, 25 °C and 45 °C ambient temperature [33].

Ambient temperature (T_{amb})	Peak error (%)		Average error (%)	
	Voltage (V)	Temperature (T)	Voltage (V)	Temperature (T)
5 °C	12.1	12.3	1.2	6.7
25 °C	5.3	6.3	0.8	1.5
45 °C	2.7	4.7	0.7	1.5

evaluated from Eq. (20). The generalised form of the model for a variable number of batteries is given by Eq. (26). The subscript (i, j) define the matrix row and coloumn respectively. The terms $R_{i,j}$ and $A_{i,j}$ are representative for non-zero arrays in the respective R and A matrices.

$$R_{i,j} = \begin{cases} 1, & i = j = 1 \\ -(R_{cell(i-1)} + R_{cell(i)} + 2R_{IC}), & i = j, \ i > 2 \\ R_{cell(\max(i,j)-1)}, & |i - j| = 1 \end{cases} \quad (26)$$

$$A_{i,j} = \begin{cases} 1, & i > 2, \ i = j \\ -1, & i > 2, \ i - j = 1 \end{cases}$$

4. Numerical coupling between Matlab and COMSOL during simulation

For an idealised operation of ESS, each battery cell connected in parallel will experience the same electrical current. This occurs when: the value of interconnect resistance (R_{IC}) equals zero or is very low when compared to the value of cell resistance; each cell has the same electrical characteristics and the ambient temperatre is constant. However, numerious studies have shown that this is not a valid assumption in the real-world [41,42], and even a small variation in resistance between cells can lead to a significant current imbalnce within the complete ESS [4,17]. To investigate cell to cell variations as a result of interconnect resistance, an electrical model of a battery pack was developed within the commercially available software package Matlab. The ESS model only includes the underpinning electrical equations of a parallel connected set of cells shown in Fig. 3 and was introduced within Section 3. As discussed in Section 2, the cell model constitutes a high fidelity electrochemical-thermal model which takes into account the temperature dependency of key electrochemical parameters. The cell model is computationaly efficient and takes circa: 30 seconds to simulate a full discarge-charge cycle uisng a desktop workstation PC (with quad-core processors (3.5 GHz) and a total random access memory (RAM) of 64 GB). As defined within the flowchart in Fig. 4, through a process of co-simulation, the two models are numerically coupled to form the complete ESS model. The flowchart that defines the operation of the simulation and execution of the model equations is presented in Fig. 4.

The input to the model is a time-varying value of current load (I_{load}). The initial condition assumes that each cell receives equal currents. Having the individual cell currents ($I_{cell,n}$) the COMSOL model runs for each cell individually and outputs, the coresponding cell resistance ($R_{cell,n}$) back to the electric cirtcuit model within Matlab. By Solving the electrical equations within Matlab a new value of current is obtained for the cell. If the current does not match the initial condition, the initial current of each cell is updated and the calculations are repetaed, as displayed in Fig. 4.

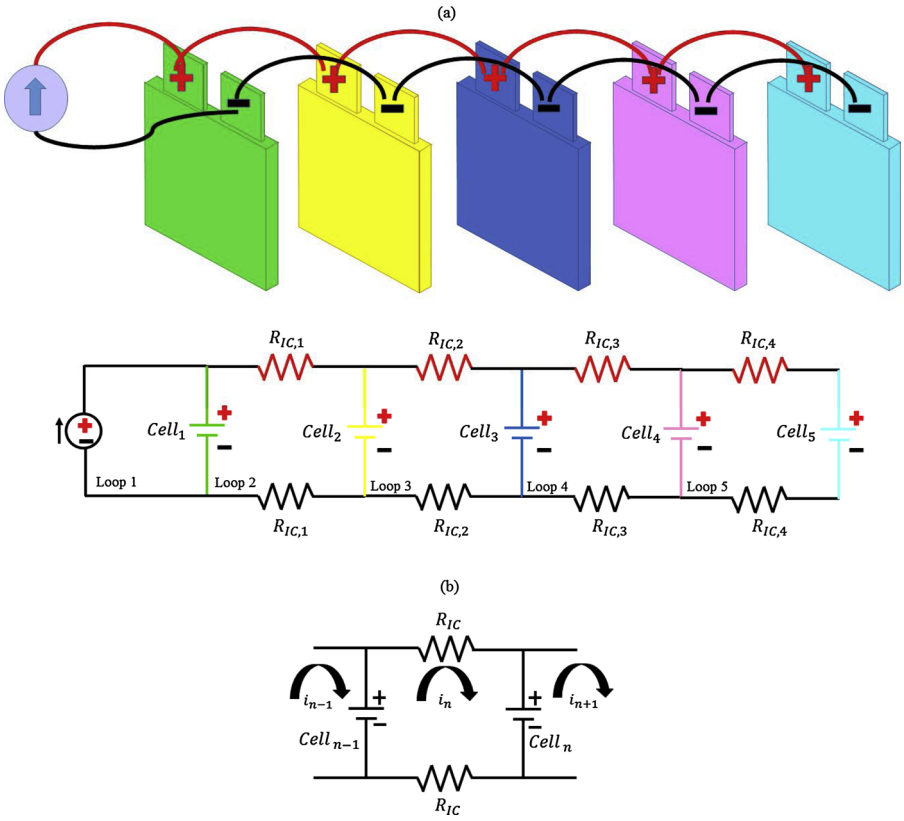

Fig. 3. (a) Schematic of a battery pack with (1S 5P) configuration, showing the interconnect resistances under an applied current source. (b) Current loop for cell *n*. Adopted from [16].

$$I_{init,cell,n} = I_{init,cell,n} + (I_{cell,n} - I_{init,cell,n})/2 \quad (27)$$

The coupled-model repeats this iterative process each time-step, at a sample interval of 10s until the simulation has completed. It is noteworthy that a 10s interval is suitable for our case, having a constant discharge current. However, the sample time would need to be reduced to circa 1s in order to emulate the current profile associated with a transient drive-cycle.

5. Results and discussion

This section presents the computational results for the different use case scenarios for the (1S-5P) parallel connection of large format 53 Ah cells.

5.1. Manufacturing tolerance of the cells

The developed cell model used in this study was extensively validated against constant charge (0.5–2*C*) and discharge current rates (0.5–5*C*) at different ambient temperatures (5–45 °C). To increase the accuracy of the measurements, all the experiments were conducted using 3 new cells placed in a thermal chamber (Weiss Gallenkamp Votsch VC3 4060). The details can be seen within [33]. The results revealed that there was a little variation in the performance of individual cells in terms of terminal voltage or achievable capacity. The capacity of the cells during discharge and charge under 5*C* (which is the most severe case), and different ambient temperatures are presented in Table 4 and Table 5respectively. The maximum capacity deviation of 2.7% is seen between cell 1 and cell 3, at 15 °C under discharge and 5 °C under constant charge condition, which can be attributed to either manufacturing inconsistency, position of the cells in the thermal chamber or measurements error. Given the small cell to cell variation, it is believed that using similar electrochemical parameters for the cells within parallel modules is a valid assumption in our case and represents a standard assumption used in the literature [1]. Modelling a parallel module with similar assumption but different approaches can also be seen within [2–6].

5.2. Different electrical loads

Inhomogeneity within key battery characteristics (of resistance and capacity) are known to be higher at larger currents. As discussed in Section 3, the ESS model comprises 5 cells connected in parallel. For the condition in which there is no interconnect resistance (R_{IC}) between the cells, each cell would perform similarly, however this assumption is known not to be valid in real world applications [16]. Within the literature there is no agreement as to a typical value for R_{IC}, as it depends on the cell size, its design and material selection. For example Wu et al. [4] reported a R_{IC} value of 0.1 mΩ to form a 12P 7S battery modules made of 4.8 Ah Kokam cells, with a resistance of 4–6 mΩ at 25 °C ambient temperature. Bruen and Marco [16] set the R_{IC} to 5 mΩ for a 4P 1S module made of cylindrical 18,650 cells with around 40 mΩ resistance at 50% SOC at 25 °C. As discussed within [10], the important factor that causes imbalances within parallel connected cells is the ratio of interconnect and cell resistance rather than the individual resistances in isolation.

The nominal resistance of the cell used in this study is 1.33 mΩ at 50% SOC, as provided by the cell manufacturer. A relative R_{IC} to R_{cell} ratio of 1–10% (corresponds to R_{IC} = 0.0133–0.133 mΩ) was set for the analysis. It is noteworthy that the actual cell resistance measured by experiments is slightly higher than the values reported by the manufacturer [33]. The performance of the 5 parallel connected cells under different electrical current loads are compared during continuous constant 1*C* and 5*C* discharge rates. A constant discharge profile can significantly reduce the computational time, which is the main reason for choosing those rather than an actual drive cycle. Further, a continuous

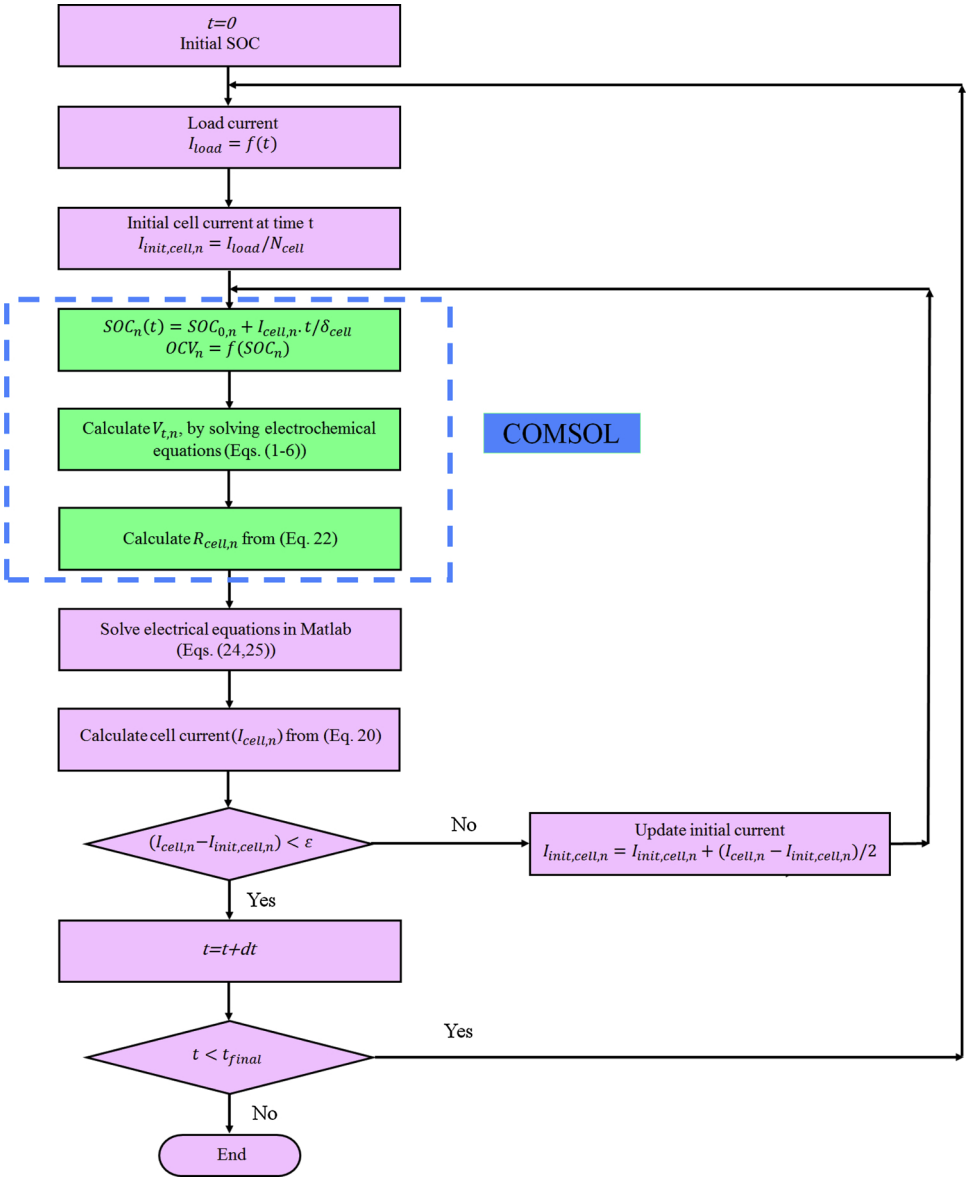

Fig. 4. The flowchart of the model operation (Matlab-COMSOL co-simulation).

Table 4
Discharge capacity of the cells under 5*C* at different ambient temperatures.

Capacity (Ah)	Ambient temperature		
	5 °C	15 °C	25 °C
Cell 1	50.05	53.51	55.55
Cell 2	50.02	53.15	55.30
Cell 3	48.79	52.03	54.68

Table 5
Charge capacity of the cells under 2*C* at different ambient temperatures.

Capacity (Ah)	Ambient temperature		
	5 °C	15 °C	25 °C
Cell 1	49.58	51.99	54.92
Cell 2	49.34	51.86	54.88
Cell 3	48.24	51.37	54.58

1*C* can be representative of a gentle duty cycle, whilst a continuous 5*C* is more replicable of an aggressive high performance EV duty cycle [43,44]. The results from this simulation are presented in Fig. 5(a) and (b). R_{IC}/R_{cell} was set to 0.01 for both cases, which is considered to be an ideal case as the ratio can exceed 0.1 as discussed within [4]. For each simulation, the cells are fully charged at the beginning of the cycles and the discharge continues until one of the cells within the parallel connection reach SOC = 0. As displayed during a 1*C* discharge, no noticeable difference is observed between the cell's performance. The current distribution among the cells largely depends on the position of the cells relative to the ESS terminals. This means that initially the cells closer to the terminals experience a higher current due to lower number of interconnect resistance they are exposed to, and the cells further from the terminals experience a lower current load due to the increased number of interconnects. As shown in [32], cell resistance is a function of SOC and increases as the SOC decreases, most notably when SOC reduces below 20%. Hence the cells with higher currents exhibit a initially higher impedance earlier than other cells, as they discharge quicker (into the 20% SOC region). When the high cell impedance compensates for their lower interconnection resistance, the situation is reversed and the cells further from the ESS terminals receive a higher

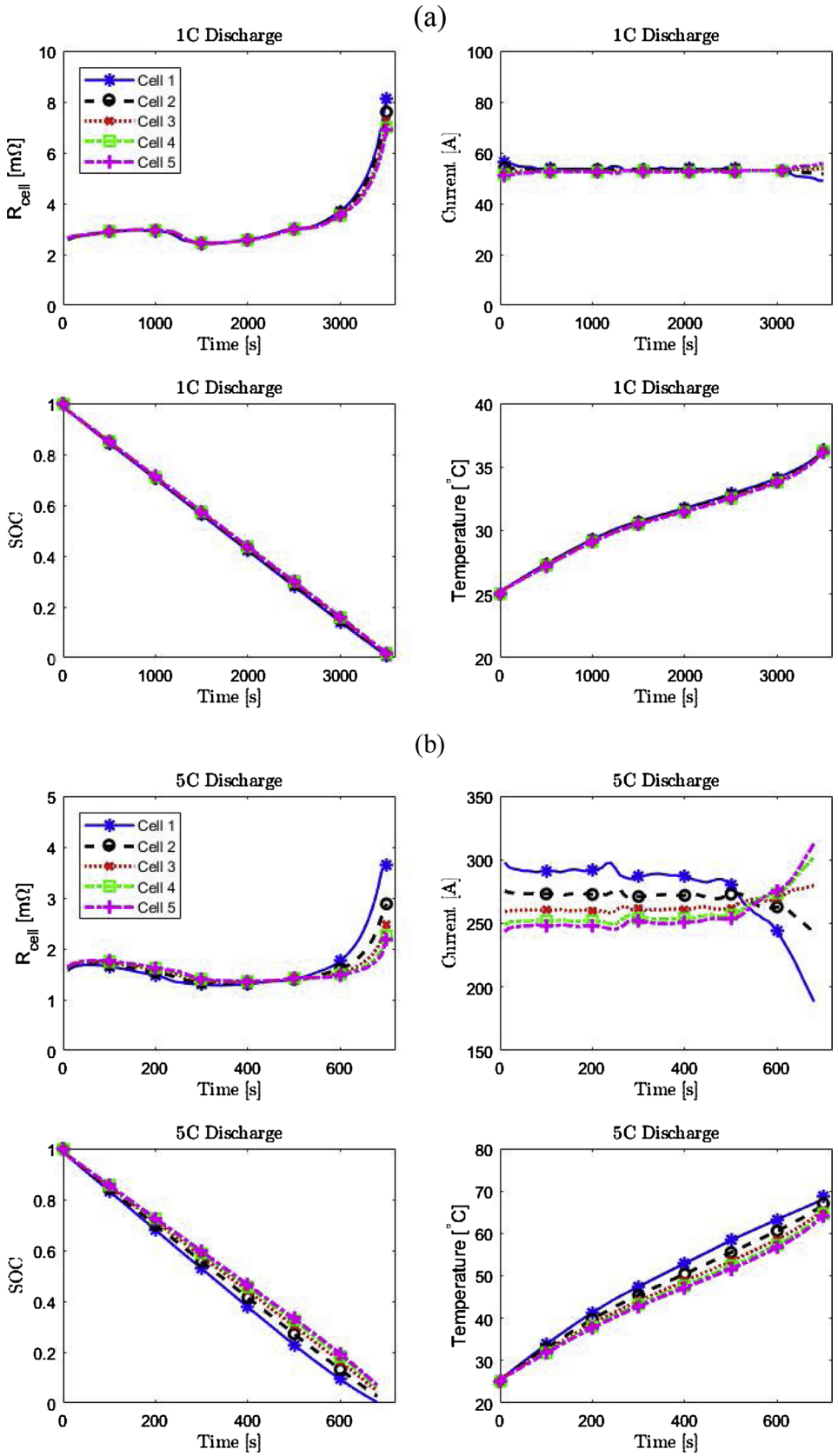

Fig. 5. Operation of the battery pack with (1S 5P) structure during 1*C* and 5*C* discharge events at 25 °C ambient temperature, $R_{IC}/R_{cell} = 0.01$.

current. This scenario is displayed in Fig. 5(a). The transition point happens after 3100s, where the cell impedances deviate from each other. The maximum current deviation between the cells is circa 11.9% at the end of discharge with average values of 3% throughout the discharge process. The maximum resistance variation is circa 18% at the end of discharge; between cell 1 and cell 5. As the current variation is

small, the maximum SOC variation is only 2% and the maximum difference between the volumetric temperature of the cells is equal to 0.4 °C which is deemed to be negligible. As the current load increases from 1*C* to 5*C* the situation changes significantly as shown in Fig. 5(b). Cell 1 initially experiences a current load 1.2 times greater than that of cell 5 and it progresses until $t = 540$ s where the peak load transition occurs between cells 1 and 5.

The maximum SOC deviation of 10% along with temperature difference of 6.9 °C is observed. However, the inconsistency within the cells tends to decrease as the current path changes. Even with such a low R_{IC}/R_{cell} ratio the temperature variation is noticeable, which may accelerate cell ageing which can further amplify the inhomogeneity after long-term operation of the pack.

5.3. Interconnect resistance and number of cells connected in parallel

By increasing the resistance ratio (R_{IC}/R_{cell}), the electrical load imbalance increases logarithmically and can lead to thermal runaway at high current loads [4] if the cells are in inadequately managed. In the case of $R_{IC}/R_{cell} = 0.1$, and during a 5*C* discharge event, the load initially experienced by cell 1 is 4 times greater than that of cell 5. The corresponding temperature rises quickly and there is insufficient time for the cells to rebalance before the discharge ends. The maximum temperature variation between the cells (ΔT_{max}) within the 1S-5P pack as a function of R_{IC}/R_{cell} is presented in Fig. 6(a). As it can be seen for a 1*C* discharge, ΔT_{max} is within an acceptable range, 4.2 °C for the worst-case scenario. However, in the case of a 5*C* discharge, the ΔT_{max} can reach 47.7 °C which is significantly high and would cause concerns at an ESS level if not managed [4]. Besides the obvious safety issue which is of considerable importance to all stakeholders, counter intuitively the results also show that the energy capacity of the pack is reduced. Due to the large current load, cell 1 discharges relatively faster than the rest of the cells and this limits the achieved capacity of the pack overall. At high interconnect resistances, especially for $R_{IC}/R_{cell} > 0.05$, this can be significantly high for both low and high *C*-rates. The available energy capacity of the pack which is not used during the 1*C* and 5*C* discharge can reach 14% and 42% respectively. At these levels, the ability of the ESS to meet key vehicle targets of driving range may be hampered, see Fig. 6(b). The figure highlights that careful consideration is necessary for a pack design specifically including high energy/high power cells connected in parallel.

Due to the existence of high interconnect resistances, a highly parallelised pack design should be avoided to ensure safety and efficient operation, as shown in Fig. 6(c). For lower electrical current loads there is less of a direct concern of inhomogeneity leading to reduced safety or system operation. However, at high electrical loads, even having 1S 3P pack leads to a high temperature variation across the cells. By increasing the number of cells from 4 to 5, the achievable energy capacity reduces. The results presented in Fig. 6 can be used as a guideline for initial pack design when evaluating different methods of cell tab connection, cell selection and ESS architecture design.

5.4. Ambient temperature

Battery performance is known to be highly dependent on ambient temperature. Temperature is known to reduce the reaction kinetics at low temperatures, conversely, the battery internal resistance increases [37,45,41]. In contrast, a lower resistance is observed at higher temperatures which is due to the improved kinetics and temperature dependency of the electrochemical parameters [45,46], which has been carefully considered for the battery model used in this study [33]. The resistance of cell 1 in the pack during a 5*C* discharge event with $R_{IC} = 0.133$ mΩ at 5, 25 and 45 °C is shown in Fig. 7(a). A higher cell resistance at low temperature, 5 °C, leads to a lower relative resistance ratio (R_{IC}/R_{cell}). This initially results in a lower current variation within the parallel connection of cells as compared to operating at higher temperatures. As the discharge progresses, the cell temperature increases, the internal resistance eventually reduces and the current inhomogeneity increases, see Fig. 7(b). The current variation is smoother for higher ambient temperatures as the cell resistance does not change significantly over the discharge time interval. The evolution of the 5 cell currents during a 5*C* discharge event at 25 °C is shown in Fig. 7(c).

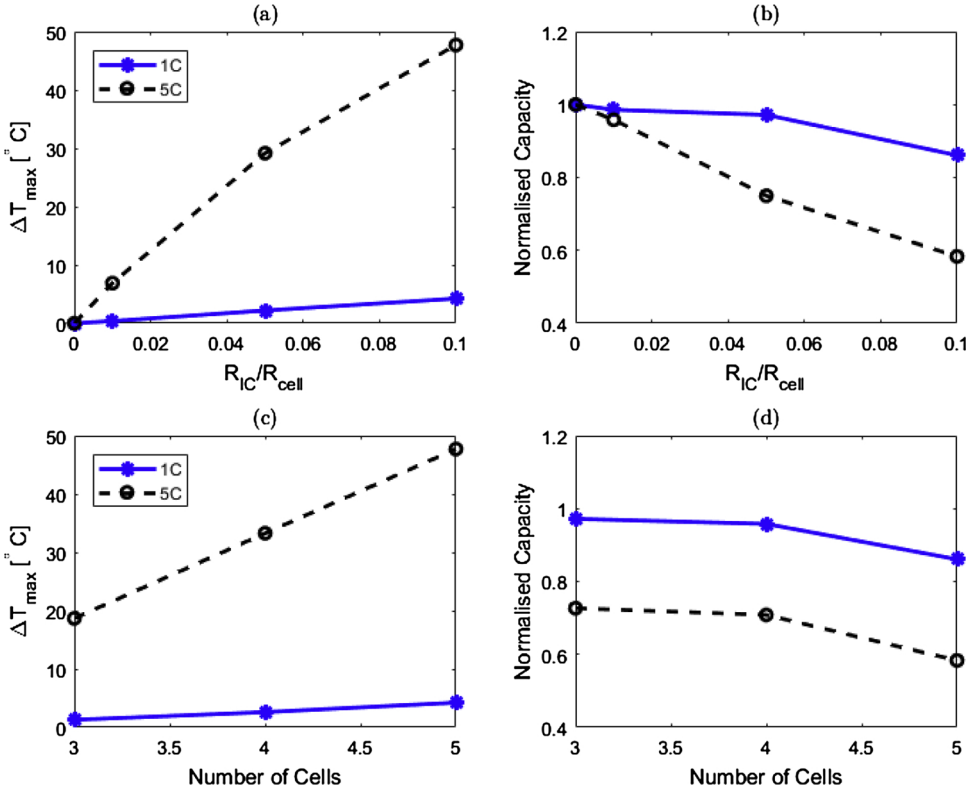

Fig. 6. (a) Average volumetric temperature variation among the cells as a function of resistance ratio. (b) Normalised capacity from the battery pack (achievable capacity of the pack relative to the pack maximum capacity in lack of interconnects), during 1*C* and 5*C* discharge events in a 1S 5P battery pack. (c) Average volumetric temperature variation among the cells as a function of parallel connected cells, (d) Normalised capacity, during 1C and 5C discharge events, $R_{IC}/R_{cell} = 0.1$.

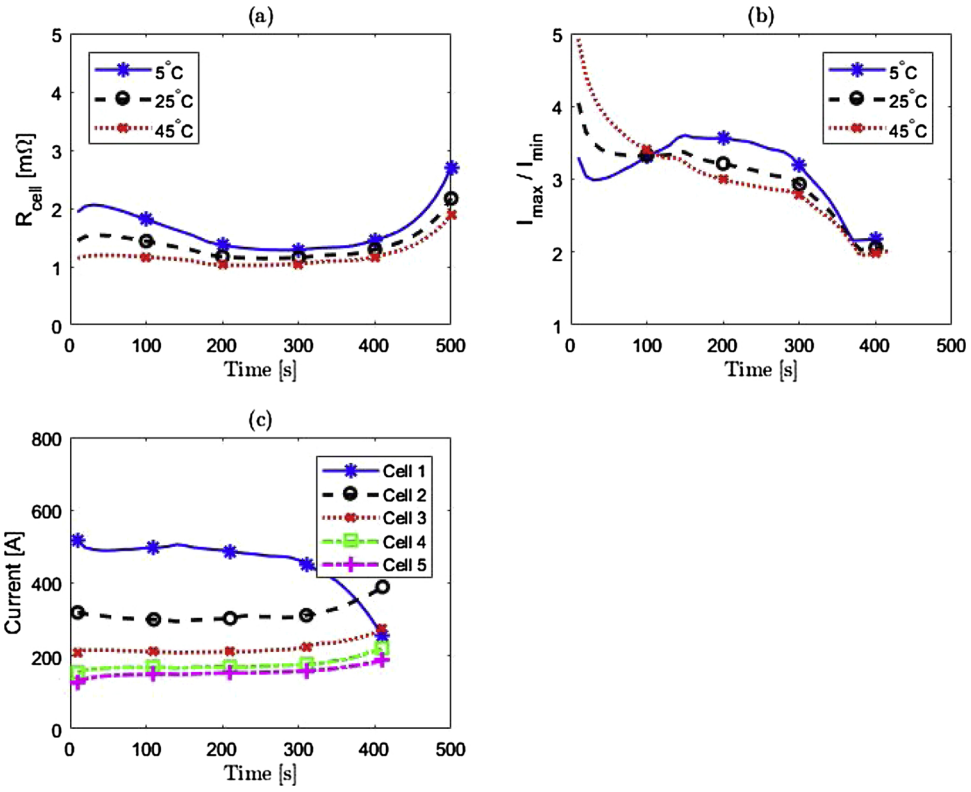

Fig. 7. (a) The resistance of cell 1 in a 1S 5P battery pack. (b) The maximum to minimum current ratio within the battery pack, during 5*C* discharge at 5 °C, 25 °C and 45 °C, R_{IC} = 0.133 mΩ. (c) Current variation of the cells during 5*C* discharge at 25 °C, R_{IC} = 0.133 mΩ.

The energy capacity reduction of the pack (the percentage of the pack capacity which is not used), and the maximum cell to cell temperature variation at different ambient temperatures as a function of resistance ratios are presented in Table 6. As shown, at lower ambient temperatures, a higher temperature variation is observed. By increasing the ambient temperature from 5 to 45 °C, ΔT_{max} is reduced by 20–26%. The capacity loss is not seen to be a strong function of temperature, but it does significantly increase as the resistance ratio increases at all ambient temperatures.

5.5. Different heat transfer coefficient for cell 1 and cell 2

The results presented so far show that for 1S 5P pack design, cells 1 and 2 which are closest to the ESS terminal experience the highest initial current loads. To reduce the inhomogeneity in current distribution for this pack design, cell 1 and cell 2 could either have a higher cell resistance or a lower interconnect resistance, so that the relative ratio of R_{IC} and R_{cell}, i.e. R_{IC}/R_{cell} decreases in line with cells 3, 4 and 5. As R_{cell} increases at lower temperature, a use case scenario including cooling conditions around cell 1 and cell 2 was investigated. Within this use case, a forced convection boundary condition is imposed around cell 1 and cell 2, with the remaining cells cooled only by natural convection. A h value of 6 $W\,m^{-2}\,K^{-1}$ was assumed for the natural convection [33], and was increased up to 3000 $W\,m^{-2}\,K^{-1}$ for a forced convection cooling. As shown in Fig. 8(a), by increasing the heat transfer coefficient (h), from 6 to 500 $W\,m^{-2}\,K^{-1}$ the cell resistance gradually increases. The new R_{IC}/R_{cell} ratio results in a slightly improved current distribution which in turn improves the achievable energy capacity of the pack by 7.1%. By further increasing the h value from 500 to 3000 $W\,m^{-2}\,K^{-1}$ the changes in both resistance and capacity are deemed to be insignificant. The SOC variation among the cells which is believed to be one of the cause of aging [9], is shown in Fig. 8(b) for a 5*C* discharge event for different h values. Similar to the cell resistance, the maximum improvement (13.5%.) is achieved for h = 500 $W\,m^{-2}\,K^{-1}$. The maximum and minimum temperature of the cells within the parallel string has been displayed in Fig. 8(c) and (d). As shown, by employing active cooling around Cell 1 and Cell 2 the maximum temperature reduces significantly to around 44 °C. While uneven cooling can slightly improve the performance of a battery pack by allowing a more uniform current distribution within the cells, it cannot be a solution in severe cases.

5.6. Unequal interconnect resistances

The results for all use case studies discussed so far are based on equal values of interconnect resistance between the cells. However, a more realistic scenario is to have different values that can represent differences in weld resistance or a possible fault condition. Table 7 presents different scenarios in which the resistance ratio varies at different locations within the pack. The Reference Case represents an equal (R_{IC}/R_{cell}) ratio of 0.01. $R_{IC,1}$ and $R_{IC,4}$ are the closest and furthest to the terminals respectively as displayed in Fig. 3. I_{min} and I_{max} are the lowest and highest initial loads within the cells during the 5*C* discharge starting from SOC = 100%. The case studies with lowest and highest

Table 6
Cell to cell temperature variation as well as capacity loss as a function of resistance ratio during a continuous 5*C* discharge at different ambient temperatures.

R_{IC}/R_{cell}	5*C*					
	ΔT_{max} (°C)			Capacity reduction (%)		
	T_{amb} = 5°C	25 °C	45 °C	T_{amb} = °C	25 °C	45 °C
0.01	8.2	6.9	6.0	4.2	4.2	4.2
0.05	34.6	29.5	26.2	26.4	25.0	25.0
0.1	56.0	47.7	44.3	43.0	42.0	41.7

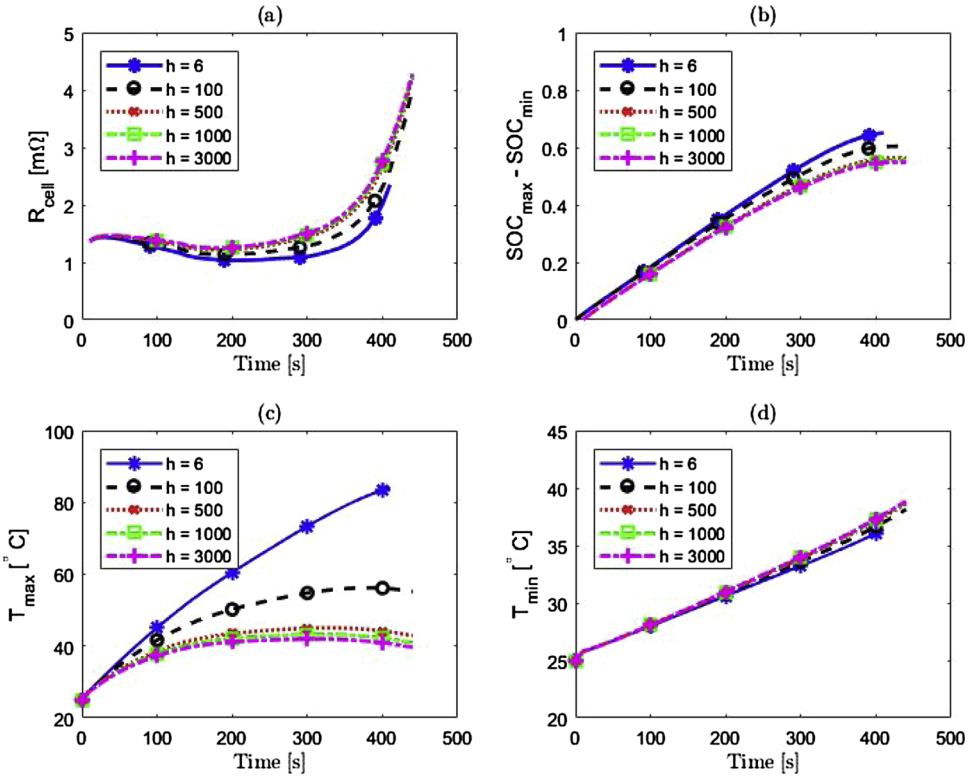

Fig. 8. (a) The resistance of cell 1, imposed to a forced convection cooling condition. (b) SOC variation between parallel cells as a function of h ($W\,m^{-2}\,K^{-1}$). (c) Maximum cell temperature within the parallel string. (d) Minimum cell temperature within the parallel string, during a 5C discharge event at 25 °C ambient temperature.

deviations between the cells are highlighted with colour codes within Table 7. The results show that, in general, unequal resistances increase the inhomogeneity within the pack. The worst-case scenario belongs to a faulty interconnect resistance close to the ESS terminals and vice versa. Having $R_{IC,1}/R_{cell} = 0.1$ increases the maximum to minimum current ratio by 73%, while having the same interconnect resistance in the furthest location from the terminal, i.e., $R_{IC,4}/R_{cell} = 0.1$, results in only a 18% increase in current variation compared to the Reference Case. This result implies that the derivation of new BMS algorithms that manage and monitor cells differently depending on their physical location within the battery system may yield improved performance and system safety.

6. Further work

The primary objective of this study was to investigate the performance limiting factors and the potential risks of employing battery packs that comprise a high number of large format cells connected in parallel. Areas of further work arising from this research are defined below.

6.1. Experimental validation and battery system ageing

The underpinning electrochemical thermal model of the lithium-ion pouch cell was experimentally validated for a range of use-cases and environmental conditions within [33]. This, combined with the application of the well-established Kirchhoff's laws for electrical circuit theory provide confidence in the results presented for the complete battery system. It is noteworthy that the results correlate well with experimental and simulation results reported in the literature [4,16]. In particular, the magnitude of the current difference that exists between the parallel connection of cells due to variations in connection impedance and also the distribution of load current between cells as batteries discharge to low values of SOC. However, for the next stage of

Table 7
Uneven interconnect resistance within the cells during the 5C discharge current and its impact on the initial load distribution.

Parameter	Ref Case	Case 1	Case 2	Case 3	Case 4	Case 5	Case 6	Case 7	Case 8
$R_{IC,1}/R_{cell}$	0.01	0.05	0.1	0.01	0.01	0.01	0.01	0.01	0.01
$R_{IC,2}/R_{cell}$	0.01	0.01	0.01	0.05	0.1	0.01	0.01	0.01	0.01
$R_{IC,3}/R_{cell}$	0.01	0.01	0.01	0.01	0.01	0.05	0.1	0.01	0.01
$R_{IC,4}/R_{cell}$	0.01	0.01	0.01	0.01	0.01	0.01	0.01	0.05	0.1
I_{min}	244	227	209	221	198	222	199	229	212
I_{max}	298	367	442	333	368	313	328	302	306
I_{max}/I_{min}	1.22	1.62	2.11	1.51	1.86	1.41	1.65	1.32	1.44
Lowest									Highest

the research a full experimental programme is required to fully validate the system level model and to expand the scope of the study. For example, to quantify the impact of cell manufacturing differences and the close-coupling that exits between load current, cell characteristics (impedance, energy capacity), ambient temperature and degradation. This initial assessment will be facilitated by the inclusion of pre-aged cells within the battery system and a temperature gradient imposed between adjacent cells within a parallel connection to quantify the resulting differential electrical loading. The longer-term impact of this on the SOH of cells connected in parallel will also be studied with the aim of reaffirming the results presented in [47], which imply that the SOH of individual cells will tend to converge to a common value.

6.2. Refinement of the battery system model

The focus of this study was to quantify the imbalance due to differences in cell interconnect resistance and cell location, further research will extend the model to include the impact of manufacturing differences between cells at the start of the simulation that may further diverge under high electrical loads and the presence of temperature gradients. Moreover, a full 3D pack model that includes the current imbalance phenomena will be created. The model will consider the interaction between the cells in order to more accurately predict the temperature evolution within the pack. Different thermal management systems will be studied to optimise ESS thermal management design and to study how to effectively remove heat from such large format cells and to keep the peak temperature and temperature gradient within the pack within an optimum range. In addition, the aim is to employ the model developed here to underpin the design of new BMS algorithms for highly parallelised systems that optimise the operation of the cells relative to their physical location within the battery assembly.

7. Conclusion

Within this study a parallel conection of 53 Ah pouch cells, with (1S-5P) configuration has been investigated. A 1D coupled electrochemical-thermal model of a cell was developed in COMSOL Multiphysics and the model was validated experimentally over a wide range of operating conditions (e.g. different charge and discharge rates, as well as different drive cycles at 5–45 °C ambient temperatures). The electrical model of the parallel connected cells was developed in Matlab. The models were numerically coupled and executed simultanously. The novelty of this model in relation to previous studies is that it takes account of the interdepenacy between cell capacity, resistance, SOC and temperature. Different use cases were investigated to highlight the potential for differential current flows within the parallel connection and the potential safety issues and hazards that emerge when using a parallel connection of cells within the battery design. The results highlight that the cell closest to the ESS terminals can reach a high temperature very rapidly which may cause thermal runaway if not properly managed. This effect is amplified as the relative ratio of interconnect resistance and cell internal resistance increases. In such cases, reducing the number of cells connected in parallel could yield supperior performance results. For example, having 4 cells instead of 5 cells in parallel is shown to improve pack performance; the acheivable energy capacity of the pack is increased by 12%. Results also show that low ambient temperatures can increase the cell to cell temperature variation. However overall, low temperatures have a greater negative impact on pack capacity. It was demonstrated how the model could be employed to underpin the analysis and design of new thermal mamnagement solutions. The scenario investigated was to cool the cells closest to the terminal to increase their internal resistance as a means of yielding a more even current distribution. However, it was observed that the increased resistance could not overcome the current imbalance created by the inclusion of the interconnect resistances within the model. The results presented highlight that a battery pack including large format cells, connected in parrellel, increases the potential risk of high peak tempereatures and gradients, espcially when the battery assembly is excited by a large electrical load. High or a faulty interconnect resistance can also cause excessive temperatures to be generated, particularly if the cause of the high resistance is physically located close to the ESS terminals.

Acknowledgements

The research was undertaken as a part of ELEVATE project (EP/M009394/1) and the Energy Storage SuperGen (EP/L019469/1) both funded by the Engineering and Physical Sciences Research Council (EPSRC).

References

[1] F.A. Lebel, S. Wilke, B. Schweitzer, M.A. Roux, S. Al-Hallaj, J.P.F. Trovao, A lithium-ion battery electro-thermal model of parallellized cells, IEEE Vehicular Technology Conference (2017) 3–8, https://doi.org/10.1109/VTCFall.2016.7880858.
[2] A.A. Pesaran, Battery thermal models for hybrid vehicle simulations, J. Power Sources 110 (2002) 377–382, https://doi.org/10.1016/s0378-7753(02)00200-8.
[3] M. Malik, I. Dincer, M. Rosen, M. Mathew, M. Fowler, Thermal and electrical performance evaluations of series connected Li-ion batteries in a pack with liquid cooling, J. Power Sources (2017) 472–481, https://doi.org/10.1016/J.APPLTHERMALENG.2017.10.029 (under revision).
[4] B. Wu, V. Yufit, M. Marinescu, G.J. Offer, R.F. Martinez-Botas, N.P. Brandon, Coupled thermal-electrochemical modelling of uneven heat generation in lithium-ion battery packs, J. Power Sources 243 (2013) 544–554, https://doi.org/10.1016/j.jpowsour.2013.05.164.
[5] L. McCurlie, M. Preindl, A. Emadi, Fast model predictive control for redistributive lithium ion battery balancing, IEEE Trans. Ind. Electron. 46 (2017) 1350–1357, https://doi.org/10.1109/TIE.2016.2611488.
[6] R. Gogoana, M.B. Pinson, M.Z. Bazant, S.E. Sarma, Internal resistance matching for parallel-connected lithium-ion cells and impacts on battery pack cycle life, J. Power Sources 252 (2014) 8–13, https://doi.org/10.1016/j.jpowsour.2013.11.101.
[7] W. Shi, X. Hu, C. Jin, J. Jiang, Y. Zhang, T. Yip, Effects of imbalanced currents on large-format $LiFePO_4$/graphite batteries systems connected in parallel, J. Power Sources 313 (2016) 198–204, https://doi.org/10.1016/j.jpowsour.2016.02.087.
[8] C. Zhang, Y. Jiang, J. Jiang, G. Cheng, W. Diao, W. Zhang, Study on battery pack consistency evolutions and equilibrium diagnosis for serial-connected lithium-ion batteries, Appl. Energy (2017), https://doi.org/10.1016/j.apenergy.2017.05.176.
[9] C. Truchot, M. Dubarry, B.Y. Liaw, State-of-charge estimation and uncertainty for lithium-ion battery packs, J. Power Sources (2013) 218–227 (submitted).
[10] G.J. Offer, V. Yufit, D.A. Howey, B. Wu, N.P. Brandon, Module design and fault diagnosis in electric vehicle batteries, J. Power Sources 206 (2012) 383–392, https://doi.org/10.1016/j.jpowsour.2012.01.087.
[11] T. Baumhöfer, M. Brühl, S. Rothgang, D.U. Sauer, Production caused variation in capacity aging trend and correlation to initial cell performance, J. Power Sources 247 (2014) 332–338, https://doi.org/10.1016/j.jpowsour.2013.08.108.
[12] M. Broussely, P. Biensan, F. Bonhomme, P. Blanchard, S. Herreyre, K. Nechev, et al., Main aging mechanisms in Li ion batteries, J. Power Sources 146 (2005) 90–96, https://doi.org/10.1016/j.jpowsour.2005.03.172.
[13] N. Yang, X. Zhang, B. Shang, G. Li, Unbalanced discharging and aging due to temperature differences among the cells in a lithium-ion battery pack with parallel combination, J. Power Sources 306 (2016) 733–741, https://doi.org/10.1016/j.jpowsour.2015.12.079.
[14] L.H. Saw, Y. Ye, A.A.O. Tay, Integration issues of lithium-ion battery into electric vehicles battery pack, J. Clean. Prod. 113 (2016) 1032–1045, https://doi.org/10.1016/j.jclepro.2015.11.011.
[15] N. Ganesan, S. Basu, K.S. Hariharan, S.M. Kolake, T. Song, T. Yeo, et al., Physics based modeling of a series parallel battery pack for asymmetry analysis, predictive control and life extension, J. Power Sources 322 (2016) 57–67, https://doi.org/10.1016/j.jpowsour.2016.05.005.
[16] T. Bruen, J. Marco, Modelling and experimental evaluation of parallel connected lithium ion cells for an electric vehicle battery system, J. Power Sources 310 (2016) 91–101, https://doi.org/10.1016/j.jpowsour.2016.01.001.
[17] M.J. Brand, M.H. Hofmann, M. Steinhardt, S.F. Schuster, A. Jossen, Current distribution within parallel-connected battery cells, J. Power Sources 334 (2016) 202–212, https://doi.org/10.1016/j.jpowsour.2016.10.010.
[18] J. Groenewald, T. Grandjean, J. Marco, Accelerated energy capacity measurement of lithium-ion cells to support future circular economy strategies for electric vehicles, Renew. Sustain. Energy Rev. 69 (2017) 98–111, https://doi.org/10.1016/j.rser.2016.11.017.
[19] X. Gong, R. Xiong, C.C. Mi, Study of the characteristics of battery packs in electric vehicles with parallel-connected lithium-ion battery cells, IEEE Trans. Ind. Appl. 51 (2014) 3218–3224.
[20] B. Wu, Z. Li, J. Zhang, Thermal design for the pouch-type large-format lithium-ion batteries: I. Thermo-electrical modeling and origins of temperature non-uniformity, J. Electrochem. Soc. 162 (2014) A181–A191, https://doi.org/10.1149/2.0831501jes.

[21] J.M. Hooper, J. Marco, G.H. Chouchelamane, C. Lyness, Vibration durability testing of nickel manganese cobalt oxide (NMC) lithium-ion 18,650 battery cells, Energies 9 (2016) 1–27, https://doi.org/10.3390/en9010052.
[22] S. Wilke, B. Schweitzer, S. Khateeb, S. Al-Hallaj, Preventing thermal runaway propagation in lithium ion battery packs using a phase change composite material: an experimental study, J. Power Sources 340 (2017) 51–59, https://doi.org/10.1016/j.jpowsour.2016.11.018.
[23] T. Wang, K.J. Tseng, J. Zhao, Z. Wei, Thermal investigation of lithium-ion battery module with different cell arrangement structures and forced air-cooling strategies, Appl. Energy 134 (2014) 229–238, https://doi.org/10.1016/j.apenergy.2014.08.013.
[24] S. Rothgang, T. Baumhöfer, H. van Hoek, T. Lange, R.W. De Doncker, D.U. Sauer, Modular battery design for reliable, flexible and multi-technology energy storage systems, Appl. Energy 137 (2015) 931–937, https://doi.org/10.1016/j.apenergy.2014.06.069.
[25] L.H. Saw, Y. Ye, A.A.O. Tay, Electro-thermal analysis and integration issues of lithium ion battery for electric vehicles, Appl. Energy 131 (2014) 97–107, https://doi.org/10.1016/j.apenergy.2014.06.016.
[26] Y. Ye, L.H. Saw, Y. Shi, K. Somasundaram, A.A.O. Tay, Effect of thermal contact resistances on fast charging of large format lithium ion batteries, Electrochim. Acta 134 (2014) 327–337, https://doi.org/10.1016/j.electacta.2014.04.134.
[27] M. Fleckenstein, O. Bohlen, M.A. Roscher, B. Bäker, Current density and state of charge inhomogeneities in Li-ion battery cells with $LiFePO_4$ as cathode material due to temperature gradients, J. Power Sources 196 (2011) 4769–4778, https://doi.org/10.1016/J.JPOWSOUR.2011.01.043.
[28] W. Zhao, G. Luo, C.-Y. Wang, Modeling internal shorting process in large-format Li-ion cells, J. Electrochem. Soc. 162 (2015) A1352–A1364, https://doi.org/10.1149/2.1031507jes.
[29] C. Veth, D. Dragicevic, C. Merten, Thermal characterizations of a large-format lithium ion cell focused on high current discharges, J. Power Sources 267 (2014) 760–769, https://doi.org/10.1016/j.jpowsour.2014.05.139.
[30] Z. Rao, S. Wang, G. Zhang, Simulation and experiment of thermal energy management with phase change material for ageing $LiFePO_4$ power battery, Energy Convers. Manage. 52 (2011) 3408–3414, https://doi.org/10.1016/j.enconman.2011.07.009.
[31] E. Hosseinzadeh, J. Marco, P. Jennings, Electrochemical-thermal modelling and optimisation of lithium-ion battery design parameters using analysis of variance, Energies 10 (2017) 1278, https://doi.org/10.3390/en10091278.
[32] E. Hosseinzadeh, J. Marco, P. Jennings, The impact of multi-layered porosity distribution on the performance of a lithium ion battery, Appl. Math. Model. 61 (2018) 107–123, https://doi.org/10.1016/j.apm.2018.04.001.
[33] E. Hosseinzadeh, R. Genieser, D. Worwood, A. Barai, J. Marco, P. Jennings, A systematic approach for electrochemical-thermal modelling of a large format lithium-ion battery for electric vehicle application, J. Power Sources 382 (2018) 77–94, https://doi.org/10.1016/j.jpowsour.2018.02.027.
[34] J. Li, Y. Cheng, L. Ai, M. Jia, S. Du, B. Yin, et al., 3D simulation on the internal distributed properties of lithium-ion battery with planar tabbed configuration, J. Power Sources 293 (2015) 993–1005, https://doi.org/10.1016/j.jpowsour.2015.06.034.
[35] S. Stewart, P. Albertus, V. Srinivasan, I. Plitz, N. Pereira, G. Amatucci, et al., Optimizing the performance of lithium titanate spinel paired with activated carbon or iron phosphate, J. Electrochem. Soc. 155 (2008) A253–A261, https://doi.org/10.1149/1.2830552.
[36] L. Zhang, C. Lyu, G. Hinds, L. Wang, W. Luo, J. Zheng, et al., Parameter sensitivity analysis of cylindrical $LiFePO_4$ battery performance using multi-physics modeling, J. Electrochem. Soc. 161 (2014) A762–A776, https://doi.org/10.1149/2.048405jes.
[37] T.R. Tanim, C.D. Rahn, C.-Y. Wang, A temperature dependent, single particle, lithium ion cell model including electrolyte diffusion, J. Dyn. Syst. Meas. Control 137 (2014) 011005, https://doi.org/10.1115/1.4028154.
[38] M. Farag, H. Sweity, M. Fleckenstein, S. Habibi, Combined electrochemical, heat generation, and thermal model for large prismatic lithium-ion batteries in real-time applications, J. Power Sources 360 (2017) 618–633, https://doi.org/10.1016/j.jpowsour.2017.06.031.
[39] M.S. Wu, C.Y. Lin, Y.Y. Wang, C.C. Wan, C.R. Yang, Numerical simulation for the discharge behaviors of batteries in series and/or parallel-connected battery pack, Electrochim. Acta 52 (2006) 1349–1357, https://doi.org/10.1016/j.electacta.2006.07.036.
[40] P. Taheri, A. Mansouri, B. Schweitzer, M. Yazdanpour, M. Bahrami, Electrical constriction resistance in current collectors of large-scale lithium-ion batteries, J. Electrochem. Soc. 160 (2013) A1731–A1740, https://doi.org/10.1149/2.041310jes.
[41] Y. Ji, Y. Zhang, C.-Y. Wang, Li-ion cell operation at low temperatures, J. Electrochem. Soc. 160 (2013) A636–A649, https://doi.org/10.1149/2.047304jes.
[42] M. Mstali, M. Farkhondeh, S. Farhad, R. Fraser, M. Fowler, Electrochemical modeling of commercial $LiFePO_4$ and graphite electrodes: kinetic and transport properties and their temperature dependence. Submitted to, J. Electrochem. Soc. 163 (2016) A2803–A2816, https://doi.org/10.1149/2.1151613jes (JESP-16-0494).
[43] D. Worwood, E. Hosseinzadeh, Q. Kellner, J. Marco, D. Greenwood, R. Mcglen, et al., Thermal analysis of a lithium-ion pouch cell under aggressive automotive duty cycles with minimal cooling, IET Hybrid and Electric Vehicles Conference (HEVC 2016) (2016) 2–3.
[44] Q. Kellner, D. Worwood, A. Barai, W.D. Widanage, J. Marco, Duty-cycle characterisation of large-format automotive lithium ion pouch cells for high performance vehicle applications, J. Energy Storage 19 (2018) 170–184, https://doi.org/10.1016/j.est.2018.07.018.
[45] Q. Wang, B. Jiang, B. Li, Y. Yan, A critical review of thermal management models and solutions of lithium-ion batteries for the development of pure electric vehicles, Renew. Sustain. Energy Rev. 64 (2016) 106–128, https://doi.org/10.1016/j.rser.2016.05.033.
[46] R.E. Gerver, 3D thermal-electrochemical lithium-ion battery computational modeling, Engineering, 2009.
[47] C. Pastor-Fernandez, T. Bruen, W.D. Widanage, M. Gama-Valdez, J. Marco, A study of cell-to-cell interactions and degradation in parallel strings: implications for the battery management system, J. Power Sources 329 (2016) 574–585.
[48] C. Zhang, J. Jiang, Y. Gao, W. Zhang, Q. Liu, X. Hu, Charging optimization in lithium-ion batteries based on temperature rise and charge time, Appl. Energy 194 (2017) 569–577.
[49] T. Liu, X. Hu, D. Cao, Reinforcement learning optimized look-ahead energy management of a parallel hybrid electric vehicle, IEEE/ASME Trans. Mechatron. 22 (4) (2017) 1497–1507.
[50] X. Hu, C. Zou, C. Zhang, Y. Li, Technical developments in batteries: a survey of principal roles, types, and management needs, IEEE Power Mag. September/October (2017).